

**UNDERSTANDING THE EFFECT OF INHIBITION ON THE TRAVELING
WAVES IN A NEURONAL NETWORK**

by

Grishma Palkar

BS-MS Dual Degree, IISER Bhopal, 2017

Submitted to the Graduate Faculty of
the Dietrich School of Arts and Sciences in partial fulfillment
of the requirements for the degree of
Master of Science

University of Pittsburgh

2020

UNIVERSITY OF PITTSBURGH
DIETRICH SCHOOL OF ARTS AND SCIENCES

This thesis was presented

by

Grishma Palkar

It was defended on

November 24, 2020

and approved by

Dr. G. Bard Ermentrout, Distinguished University Professor

Dr. Jonathan Rubin, Professor and Department Chair

Dr. David Swigon, Associate Professor

Thesis Advisor: Dr. G. Bard Ermentrout, Distinguished University Professor

Copyright © by Grishma Palkar

2020

UNDERSTANDING THE EFFECT OF INHIBITION ON THE TRAVELING WAVES IN A NEURONAL NETWORK

Grishma Palkar, M.S.

University of Pittsburgh, 2020

We study the effect of inhibition on the traveling waves arising in neuronal network. A neuronal firing rate model of sensory cortex has two population types, excitatory and inhibitory. We are interested in the case when we have three fixed points: (1) a stable down state; (2) a saddle point with stable manifold that acts as a threshold for firing; (3) an up state. We will look at the case when the upstate is unstable, which gives rise to pulse (a transient increase in firing that returns to the down state). We will first study the effects of inhibition on the spiking neuronal model. Then we will reduce the spiking neuronal model to a Wilson-Cowan like equations and try to mimic the results that we obtained in the original spiking model. In the Wilson-Cowan equations, we first look at the model with smooth firing rate function and later with Heaviside firing rate function. In the Heaviside firing rate case, we investigate the existence of the traveling wave and study the stability using the Evans-function (a complex analytic function obtained by linearizing a system about its traveling wave and whose zeros give the eigenvalues of the linearized operator). The Evans function allows us to study the stability of a given wave and identify bifurcation points (loss of stability) as the spatial extent of inhibition is varied. We observe an Andronov-Hopf bifurcation and later we explore the behavior of the traveling waves as the spatial scales of the inhibition population change and notice oscillatory instability.

TABLE OF CONTENTS

PREFACE	ix
1.0 INTRODUCTION	1
1.1 Spiking neuronal model	3
1.2 Firing rate of the QIF model	7
1.3 The Wilson-Cowan equations: excitatory - inhibitory model with adaptation	8
1.3.1 The phase plane and equilibria	9
2.0 SPATIALLY DISTRIBUTED NETWORK OF WILSON-COWAN EQUATIONS	12
2.1 The Wilson-Cowan model with smooth firing rate function	13
3.0 WILSON-COWAN EQUATIONS WITH HEAVISIDE FIRING RATE FUNCTION	21
3.1 Existence of the traveling wave solution	21
3.2 Stability analysis of Wilson-Cowan equations with Heaviside firing rate function	26
3.2.1 Evans function	30
4.0 Conclusions	36
BIBLIOGRAPHY	37

LIST OF TABLES

1	Table of parameter values for the spiking neuronal model.	6
2	Table of parameter values for system (1.8).	11

LIST OF FIGURES

1	(a) Neuron and myelinated axon, with signal flow from inputs at dendrites to outputs at axon terminals. (d) A neuronal action potential ("spike"). Note that the amplitude and the exact shape of the action potential can vary according to the exact experimental technique used for acquiring the signal.	2
2	(a) $g_{ei} = 0.1$,(b) $g_{ei} = 0.2$. We observe as g_{ei} increases lesser number of neurons fire.	4
3	(c) $g_{ei} = 0.4$,(d) $g_{ei} = 0.8$. We observe as g_{ei} increases lesser number of neurons fire.	5
4	(a) u - v phase plane with $g_a = 0$, (b) u - z phase plane with $g_{ei} = 0$, (c) u , v , z versus t	10
5	(a) Plot of K_e and K_i with $\sigma_i = 0.5$ and $\sigma_i = 1.5$ (b) $F(x) = 1/(1 + e^{-shp \cdot x})$ with increasing gain parameter: $shp = [1, 4, 10]$. For large value of shp , $F(x)$ can be approximated by the Heaviside function.	14
6	Schematic diagram of the spatially distributed network of the Wilson-Cowan equations.	15
7	Space-time plot of the excitatory population with the smooth firing rate function for (a) $g_{ei} = 5$ and (b) $g_{ei} = 15$	16
8	Figure (i) vel/g_{ei} , (ii) vel/τ_i , (iii) vel/σ_i , (iv) vel/g_a , (v) vel/d_e and (vi) vel/d_i are the velocity plots for smooth firing rate function (red curve) and Heaviside firing rate function (blue curve).	17
9	Figure (i) $width/g_{ei}$, (ii) $width/\tau_i$, (iii) $width/\sigma_i$, (iv) $width/g_a$, (v) $width/d_e$ and (vi) $width/d_i$ are the width plots for smooth firing rate function (red curve) and Heaviside firing rate function (blue curve).	18
10	Homoclinic orbits in the u - v phase plane for (a) varying g_{ei} ,(b) varying σ_i and (c) varying τ_i	19
11	Space-time plot of the excitatory population with the Heaviside firing rate function for (a) $g_{ei} = 5$ and (b) $g_{ei} = 15$	22

12	u_{100} versus t (green), v_{100} versus t (red), z_{100} versus t (blue) plots. Scaled so that u_{100} starts at zero.	24
13	Plot of real and imaginary parts of the Evans function $\mathcal{E}(\beta)$ for the model with (a) $\sigma_i = 1.49$, (b) $\sigma_i = 1.502$ and (c) $\sigma_i = 1.52$ respectively. This illustrates a possibility of a dynamic instability with increasing σ_i as a pair of complex eigenvalues cross over to the right-hand plane through the imaginary axis. Figure (d) is the plot of Real part and Imaginary part of a root (green circle) of the Evans function vs σ_i . The graph of real part of Evans function crosses zero at approximately $\sigma_i = 1.5$	33
14	Space-time plot of the excitatory population with the Heaviside firing rate for (a) $\sigma_i = 0.5$, (b) $\sigma_i = 1.467$ and (c) $\sigma_i = 1.47$	34
15	Space-time plot of the excitatory population with the smooth firing rate function for (a) $\sigma_i = 0.5$, (b) $\sigma_i = 1.566$ and (c) $\sigma_i = 1.574$	35

PREFACE

The author would like to especially acknowledge her advisor Dr. Bard Ermentrout and the University of Pittsburgh for their time, energy, guidance and resources. The author would like to thank her family for their constant encouragement and support.

1.0 INTRODUCTION

Spiking neural networks (SNNs) are artificial neural networks that more closely mimic natural neural network . In SNNs, each neuron, it's membrane potential and synapses are represented. The idea is that neurons in the SNN transmit information only when a membrane potential reaches a specific value, called the threshold. When the membrane potential reaches the threshold, the neuron fires, and generates a signal ('spike') that travels to other neurons which, in turn, increase or decrease their potentials in response to this signal. A neuron model that fires at the moment of threshold crossing is also called a spiking neuron model.

The most prominent spiking neuron model is the integrate-and-fire model. In the integrate-and-fire model, the incoming spiking input pushes the neuron's membrane potential to a value higher or lower, until the state eventually either decays or if the firing threshold is reached, the neuron fires. After firing, the state variable is reset to a lower value. In our work we would be using the quadratic integrate and fire (QIF) model. A quadratic integrate and fire neuron is defined by the autonomous differential equation,

$$\frac{dx}{dt} = x^2 + I$$

where I is a real positive constant. A solution to this differential equation is the tangent function, which blows up in finite time. Thus a "spike" is said to have occurred when the solution reaches positive infinity, and the solution is reset to negative infinity.

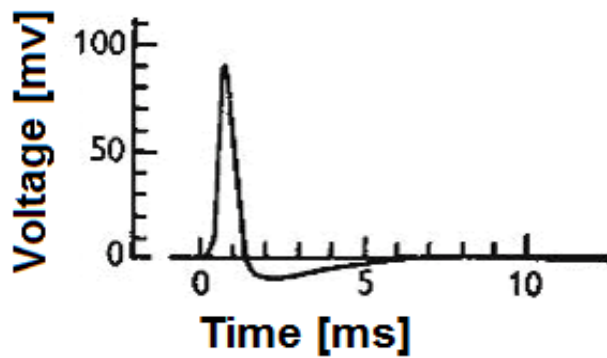
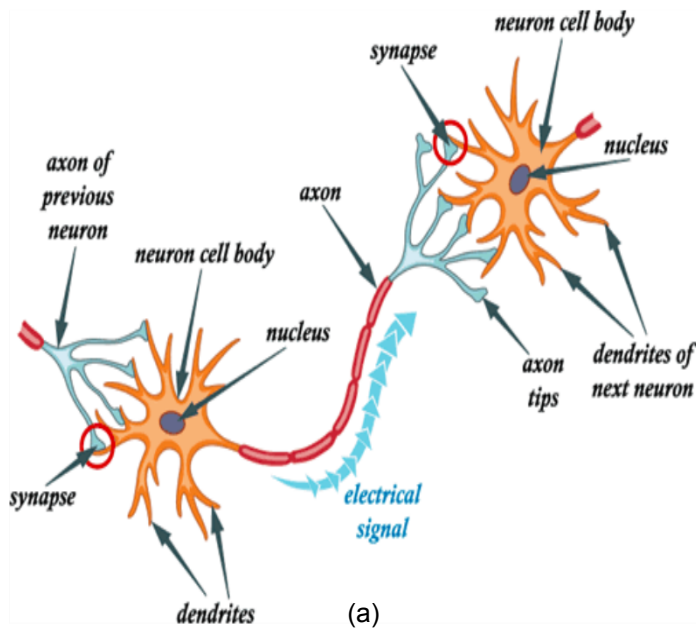


Figure 1: (a) Neuron and myelinated axon, with signal flow from inputs at dendrites to outputs at axon terminals. (d) A neuronal action potential ("spike"). Note that the amplitude and the exact shape of the action potential can vary according to the exact experimental technique used for acquiring the signal.

1.1 Spiking neuronal model

We will consider the following neuronal model:

$$c_m \frac{du}{dt} = \frac{g_l(u - E_r)(u - E_{th})}{E_{th} - E_r} + I_u - g_{ad}z(v - E_k) - g_{ei}s_i(u - I_{syn}) - g_{ee}s_e(u - E_{syn}) \quad (1.1)$$

$$c_m \frac{dv}{dt} = \frac{g_l(v - E_r)(v - E_{th})}{E_{th} - E_r} + I_v - g_{ie}s_e(v - E_{syn}) - g_{ii}s_i(v - I_{syn}) \quad (1.2)$$

$$\frac{dz}{dt} = \frac{-z}{\tau_z} + \frac{\delta(u - u_{spike})}{\tau_z} \quad (1.3)$$

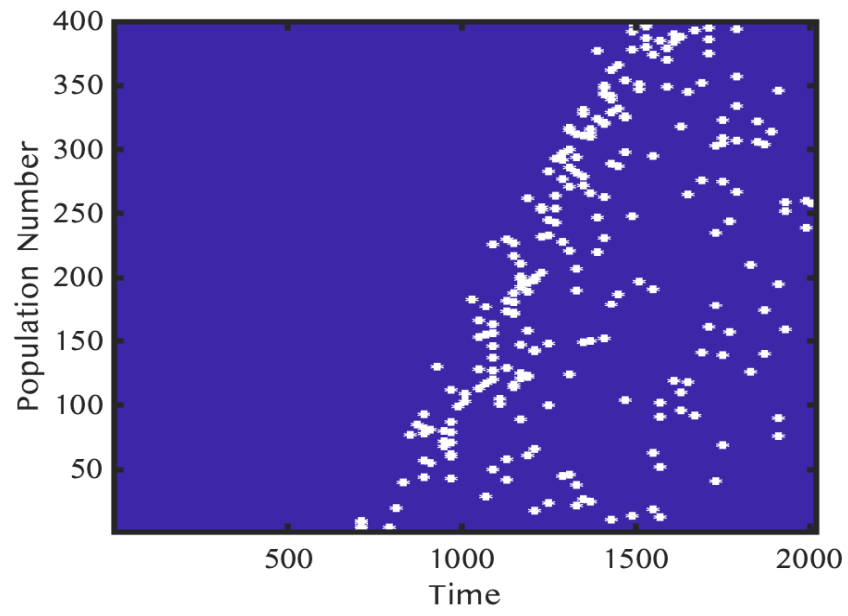
$$\frac{ds_e}{dt} = \frac{-s_e}{\tau_e} + \frac{\delta(u - u_{spike})}{\tau_e} \quad (1.4)$$

$$\frac{ds_i}{dt} = \frac{-s_i}{\tau_i} + \frac{\delta(v - v_{spike})}{\tau_i} \quad (1.5)$$

Where u, v are firing rates of excitatory and inhibitory populations, respectively. s_e, s_i are excitatory and inhibitory synaptic terms respectively. Equation (1.3) is the equation for adaptation (z). The parameters g_{jk} are coupling strengths from population k to population j ; $j, k \in \{e, i\}$. The parameters τ_e, τ_i, τ_z represent the time scales of the excitation, inhibition and adaptation, respectively. E_{th} and E_r are the threshold and rest voltages, respectively. E_k is the reversal potential for K^+ . Here c_m is the membrane capacitance, g_l is leak conductance, g_{ad} is the strength of adaptation and I_u and I_v are the excitatory and inhibitory input currents, respectively. E_{syn} and I_{syn} are excitatory and inhibitory synaptic reversal potentials, respectively. When u spikes i.e. $u = u_{spike}$ (eq. (1.3) and (1.4)) z and s_e are incremented by $\frac{1}{\tau_z}$ and $\frac{1}{\tau_e}$, respectively. When $v = v_{spikes}$ (eq. 1.5), s_i is incremented by $\frac{1}{\tau_i}$. We want to study the effects of inhibition on the spiking of the neurons.

To better study this effect we reduce the equations in the spiking neuronal model to a simpler Wilson-Cowan equations. In the later chapter we will look at the Wilson-Cowan equations with smooth firing rate and Heaviside firing rate functions and observe that the traveling wave arising in the excitatory population show similar behavior to inhibition as the spiking model.

(a) $g_{ei} = 0.1$



(b) $g_{ei} = 0.2$

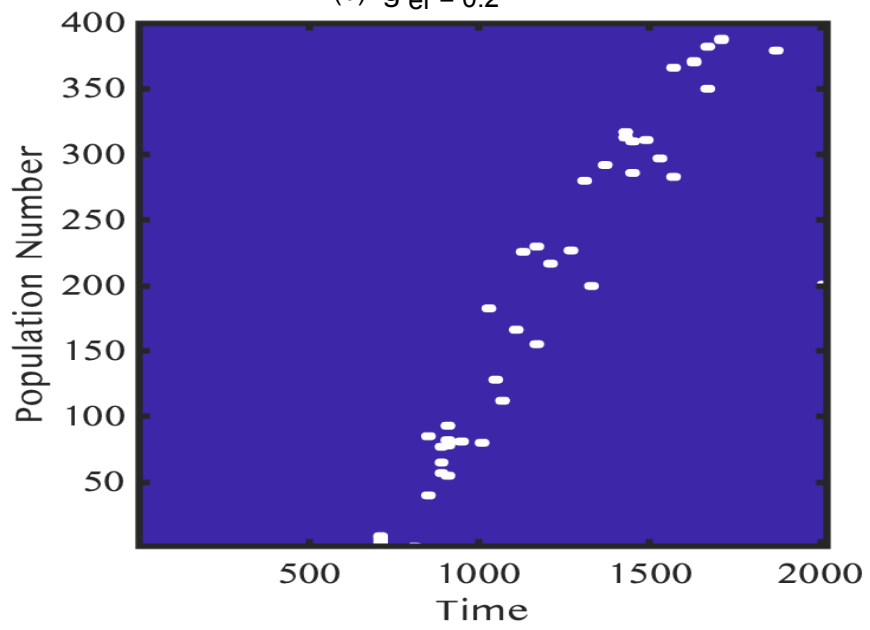


Figure 2: (a) $g_{ei} = 0.1$,(b) $g_{ei} = 0.2$. We observe as g_{ei} increases lesser number of neurons fire.

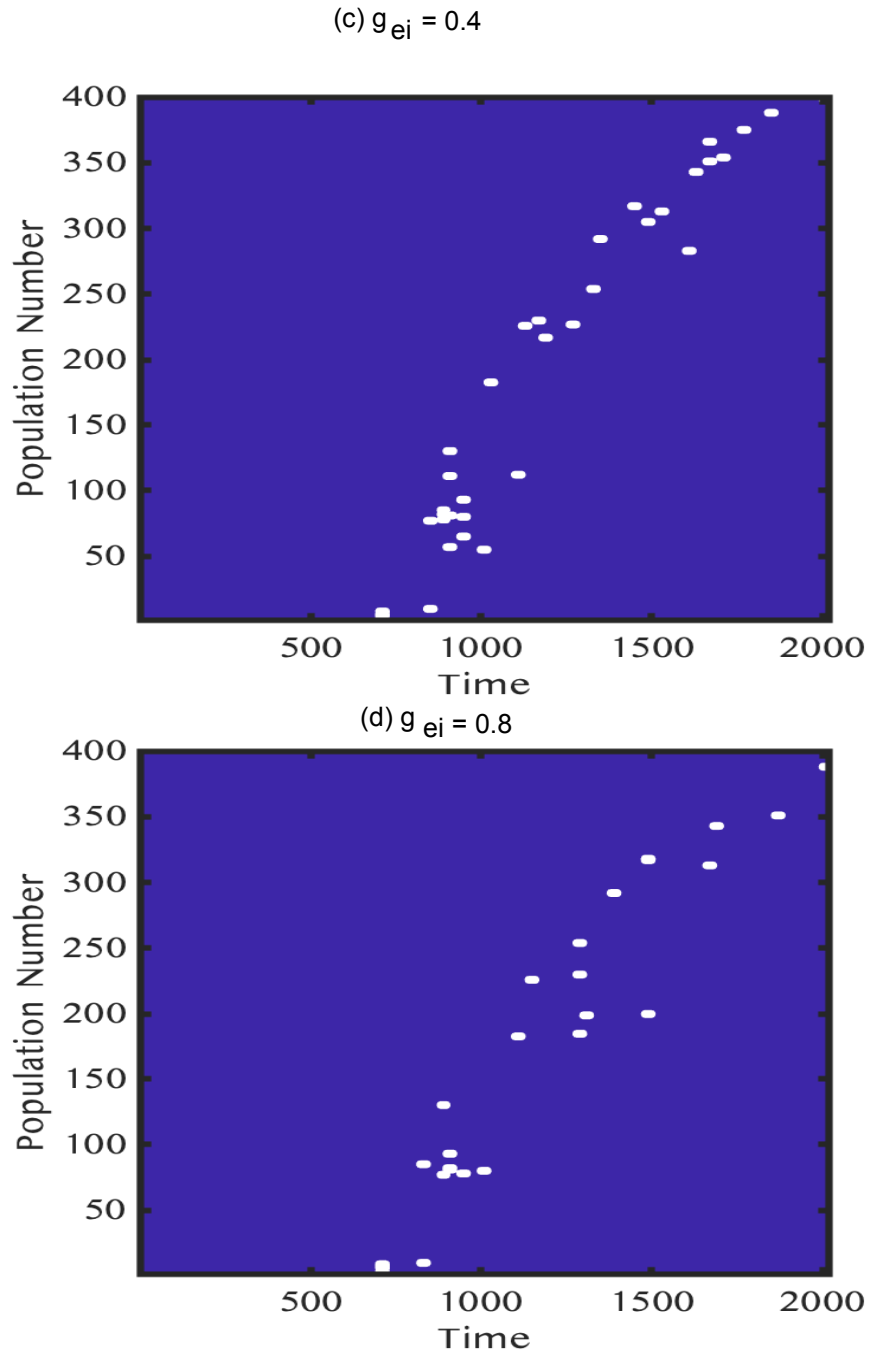


Figure 3: (c) $g_{ei} = 0.4$, (d) $g_{ei} = 0.8$. We observe as g_{ei} increases lesser number of neurons fire.

Parameters	Values
g_{ei}	0.4
g_{ee}	0.1
g_{ie}	0.1
g_{ii}	0.1
g_{ad}	0.1
τ_e	3
τ_z	50
τ_i	4
c_m	1
g_l	0.1
E_r	-70
E_{th}	-50
E_k	-85
E_{syn}	0
I_{syn}	-75

Table 1: Table of parameter values for the spiking neuronal model.

1.2 Firing rate of the QIF model

Equation (1.1) and (1.2) for excitatory and inhibitory population respectively, can be rearranged to obtain the following general differential equation:

$$\frac{df}{dt} = Cf^2 + Bf + A \quad (1.6)$$

For equation (1.1) $f = u$ and we have,

$$A = a_e(s_e, s_i, z) = \frac{1}{c_m} \left[\frac{g_l E_r E_{th}}{(E_{th} - E_l)} + I_u + g_{ad} z E_k + g_{ei} s_i I_{syn} + g_{ee} s_e E_{syn} \right]$$

$$B = b_e(s_e, s_i, z) = \frac{-1}{c_m} \left[\frac{g_l (E_{th} + E_r)}{E_{th} - E_r} + g_{ad} z + g_{ei} s_i + g_{ee} s_e \right]$$

for equation (1.2) $f = v$ and we have,

$$A = a_i(s_e, s_i, z) = \frac{1}{c_m} \left[\frac{g_l E_r E_{th}}{(E_{th} - E_l)} + I_v + g_{ie} s_e E_{syn} + g_{ii} s_i I_{syn} \right]$$

$$B = b_i(s_e, s_i, z) = \frac{-1}{c_m} \left[\frac{g_l (E_{th} + E_r)}{E_{th} - E_r} + g_{ii} s_i + g_{ie} s_e \right];$$

and

$$C = \frac{g_l}{c_m (E_{th} - E_r)}$$

for both the equations.

Integrating equation (1.6) from $V_{reset} = -\infty$ to $V_{spike} = +\infty$, we have T , the time period of spiking as

$$T = \frac{\pi}{C\alpha}$$

where $\alpha = \sqrt{\frac{4AC - B^2}{4C^2}}$.

Hence, the firing rate, $f = \frac{1}{T} = \frac{\sqrt{4AC - B^2}}{2\pi}$.

In particular, the firing rate for excitatory (1.1) populations is given by

$$f_e(s_e, s_i, z) = \frac{\sqrt{4a_e(s_e, s_i, z)C - b_e(s_e, s_i, z)^2}}{2\pi}$$

and the firing rate for inhibitory (1.2) populations is given by

$$f_i(s_e, s_i, z) = \frac{\sqrt{4a_i(s_e, s_i, z)C - b_i(s_e, s_i, z)^2}}{2\pi}$$

Thus, we can reduce the spiking model to Wilson-Cowan like model with adaptation :

$$\begin{aligned}
\tau_e s_e' &= -s_e + f_e(s_e, s_i, z) \\
\tau_i s_i' &= -s_i + f_i(s_e, s_i, z) \\
\tau_z z' &= -z + f_e(s_e, s_i, z)
\end{aligned} \tag{1.7}$$

We will now study the Wilson-Cowan equations. The Wilson-Cowan equations are set so that it fits the above reduced spiking model i.e. we can fit the nullclines, have the same number of fixed points and the trajectories match. First, we will look at the Wilson-Cowan equations with a smooth firing rate function.

1.3 The Wilson-Cowan equations: excitatory - inhibitory model with adaptation

Let us consider a model of interacting excitatory (u) and inhibitory (v) populations along with adaptation (z) given by

$$\begin{aligned}
u' &= -u + \frac{1}{p} f(p \cdot g_{ee} \cdot u - q \cdot g_{ei} \cdot v - \theta_e - g_a \cdot z) \\
v' &= (-v + \frac{1}{q} f(p \cdot g_{ie} \cdot u - q \cdot g_{ii} \cdot v - \theta_i)) / \tau_i \\
z' &= (-z + f(p \cdot a_{ze} \cdot u - \theta_z)) / \tau_z
\end{aligned} \tag{1.8}$$

where $' = \frac{d}{dt}$, f is the firing rate function, $f(x) = \frac{1}{(1+e^{-shp \cdot x})}$ and shp is the gain parameter that modulates the steepness of the curve. The time-scale of excitation is taken to be one, τ_i is the time scale of inhibition relative to excitation, τ_z is the time scale of adaptation relative to excitation, θ_e , θ_i and θ_z are the thresholds for u , v and z , respectively. $p = 21$ and $q = 8$ are the scaling factors chosen so that the nullclines for the systems (1.7) and (1.8) match. The parameters g_{jk} are coupling strengths from population k to population j ; $j, k \in \{e, i\}$, g_a is the strength of adaptation, a_{ze} is the coupling strength between the excitation and adaptation. Now let us look at the nullcline structure and the phase plane.

1.3.1 The phase plane and equilibria

We study the phase plane of the excitation-inhibition system and excitation-adaptation system in system (1.8). In our setup, we consider set of parameters so that there are three equilibria: the stable down state; a saddle point with stable manifold that acts as a threshold for firing; and the up state. We use the parameter values from table (2) for this model and all the later models. In Fig(4a), we see the $u - v$ nullclines, the excitatory-inhibitory system with adaptation equal to zero ($g_a = 0$) in (1.8), which satisfy

$$\begin{aligned} 0 &= -u + \frac{1}{p}f(p \cdot g_{ee} \cdot u - q \cdot g_{ei} \cdot v - \theta_e - g_a \cdot z) \\ 0 &= (-v + \frac{1}{q}f(p \cdot g_{ie} \cdot u - q \cdot g_{ii} \cdot v - \theta_i))/\tau_i \end{aligned} \quad (1.9)$$

and in Fig(4b), we see the $u - z$ nullclines for system (1.8) with inhibition equal to zero ($g_{ei} = 0$), which satisfy

$$\begin{aligned} 0 &= (-v + \frac{1}{q}f(p \cdot g_{ie} \cdot u - q \cdot g_{ii} \cdot v - \theta_i))/\tau_i \\ 0 &= (-z + f(p \cdot a_{ze} \cdot u - \theta_z))/\tau_z \end{aligned} \quad (1.10)$$

In fig(4a) and fig(4b) the down state is denoted by a blue circle, the saddle point is denoted by a yellow star and the up state is denoted by a green square. We observe that the choice of parameters we made guarantees that the up state is unstable and hence we obtain homoclinic orbits. If the spiking input is large enough to make the neuron's membrane potential cross the threshold, the neuron fires. After which the inhibition comes into play and it brings the neuron back to rest. For fig(4c) we see that when $g_{ei} = 0$ i.e. inhibition is off, u stays on for a very long time compared to when adaptation (g_a) is off. In the next chapter we will extend the model (1.8) to include spatially-dependent connections.

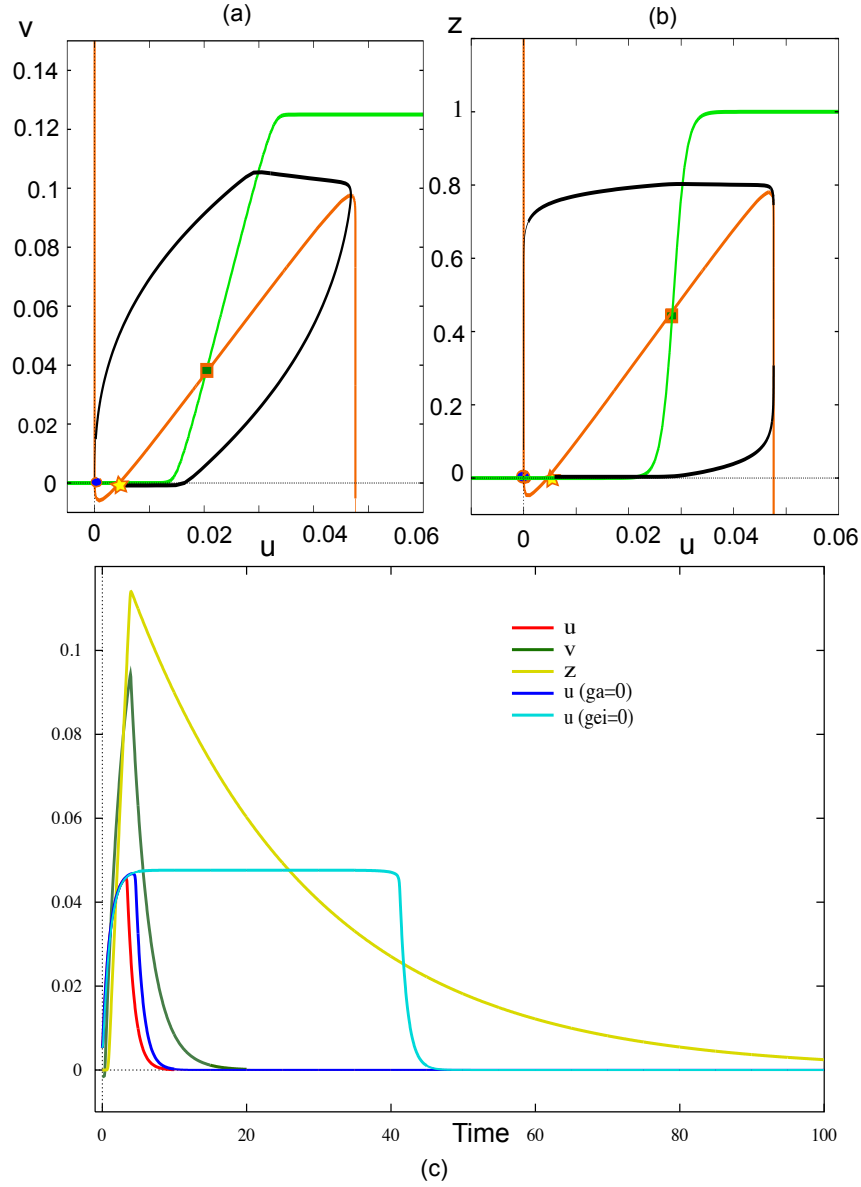


Figure 4: (a) u - v phase plane with $g_a = 0$, (b) u - z phase plane with $g_{ei} = 0$, (c) u , v , z versus t .

Parameters	Values
g_{ei}	15
g_{ee}	15
g_{ie}	25
g_{ii}	8
g_a	15
a_{ze}	10
θ_e	2
θ_i	8.5
θ_z	6
τ_z	25
τ_i	2.5
p	21
q	8

Table 2: Table of parameter values for system (1.8).

2.0 SPATIALLY DISTRIBUTED NETWORK OF WILSON-COWAN EQUATIONS

Large networks of synaptically connected neurons are often modeled by so-called firing rate or neural field equations, typically with two types of populations: excitatory (u) and inhibitory (v). Wilson-Cowan equations are one such type of neuronal field equations. The model was developed by Hugh R. Wilson and Jack D. Cowan. Key parameters in the model are the strength of connectivity between each sub-type of population (excitatory and inhibitory). Varying these parameters we generate diverse dynamical behaviors that are represent the observed activity in the brain, like multi-stability, oscillations, traveling waves and spatial patterns. We extend this model of cortex to include spatially-dependent connections.

$$\frac{\partial u}{\partial t}(x, t) = -u(x, t) + \frac{1}{p}F(p \cdot d_e \cdot g_{ee} \cdot K_e(x) * u(x, t) \quad (2.1)$$

$$\begin{aligned} & - q \cdot d_i \cdot g_{ei} \cdot K_i(x) * v(x, t) - g_a \cdot z - \theta_e \\ \tau_i \frac{\partial v}{\partial t}(x, t) & = -v(x, t) + \frac{1}{q}F(p \cdot d_e \cdot g_{ie} \cdot K_e(x) * u(x, t) \quad (2.2) \end{aligned}$$

$$\begin{aligned} & - q \cdot d_i \cdot g_{ii} \cdot K_i(x) * v(x, t) - \theta_i \\ \tau_z \frac{\partial z}{\partial t}(x, t) & = -z(x, t) + F(p \cdot a_{ze} \cdot u(x, t) - \theta_z) \quad (2.3) \end{aligned}$$

where u, v are the firing rates of the excitatory and inhibitory populations, respectively and z is the adaptation equation. $K_j(x)$, $j \in \{e, i\}$ are spatial interaction Gaussian functions which are convolved with the activities. Here, $k(x) * m(x) := \int_D k(x-y)m(y)dy$, where D is the spatial domain of the network. The parameters τ_j , $j \in \{e, i, z\}$ represent synaptic time constants; the parameters g_{jk} are the coupling strengths from population k to population j and θ_j are thresholds. $F(I)$ is a nonlinear function representing the firing rate as a function of the spatially distributed inputs. Since we can re-scale time, without loss of generality, we set $\tau_e = 1$, so that τ_i is the relative time constant of inhibition to excitation. The parameters p and q are the scaling factors and are chosen to be 21 and 8 respectively to match the s_e - s_i nullclines in system (1.7). Parameters d_e and d_i measure the strength of excitation and

inhibition, respectively. The parameters $\sigma_j, j \in \{e, i\}$ are the spatial scales of the excitatory and inhibitory connections. We set $\sigma_e = 1$ and σ_i is the ratio of the spatial scale of inhibition relative to excitation.

$$K_e(x) = \frac{\exp(-(\frac{x}{\sigma_e})^2)}{\sqrt{\pi}\sigma_e}, K_i(x) = \frac{\exp(-(\frac{x}{\sigma_i})^2)}{\sqrt{\pi}\sigma_i}$$

normalized so that $\int_R K_e(x)dx = \int_R K_i(x)dx = 1$. (Fig5a)

2.1 The Wilson-Cowan model with smooth firing rate function

In this section we consider the smooth firing rate function $F(I) = \frac{1}{(1+e^{-4I})}$. We are interested in understanding the effect of inhibition on the traveling wave. We analyse the traveling wave arising in the excitatory population as we changed g_{ei} . Fig(7) depicts that as we increase inhibition (g_{ei}), the amount of time for which a neuron fires decreases. This agrees with the observation from the spiking model.

Next, we study how velocity of the traveling wave depends on the parameters such as $g_{ei}, \sigma_i, \tau_i, g_a, d_e, d_i$. We take $velocity = 50/max(1, t_{150} - t_{100})$, where t_{100} is the time at which u_{100} crosses the u threshold ($u_{th} = 0.01$) from below and t_{150} is the time at which u_{150} crosses the u threshold from below. The plots for velocity versus $g_{ei}, \sigma_i, \tau_i, g_a, d_e, d_i$ are computed using the data obtained from xppaut by integrating and ranging over the desired parameter.

Now, lets look at the figure(8) and study how the velocity (red curve) behaves as we vary parameters. Velocity of a traveling wave is determined by excitation until inhibition gets stronger. We observe velocity (red curve) decreases gradually with increasing g_{ei} (Fig8i), σ_i (Fig8iii) and d_i (Fig8iv). This is because as the strength of inhibition increases it becomes more difficult for the next neuron to fire, which leads to a decrease in the velocity of the wave.

Velocity (red curve) increases with increasing τ_i (Fig8ii). As τ_i increases the time it takes for the inhibition to come on increases and so there is more excitation. Hence velocity increases steeply until inhibition comes on (which is around $\tau_i = 2.5$) and after that it

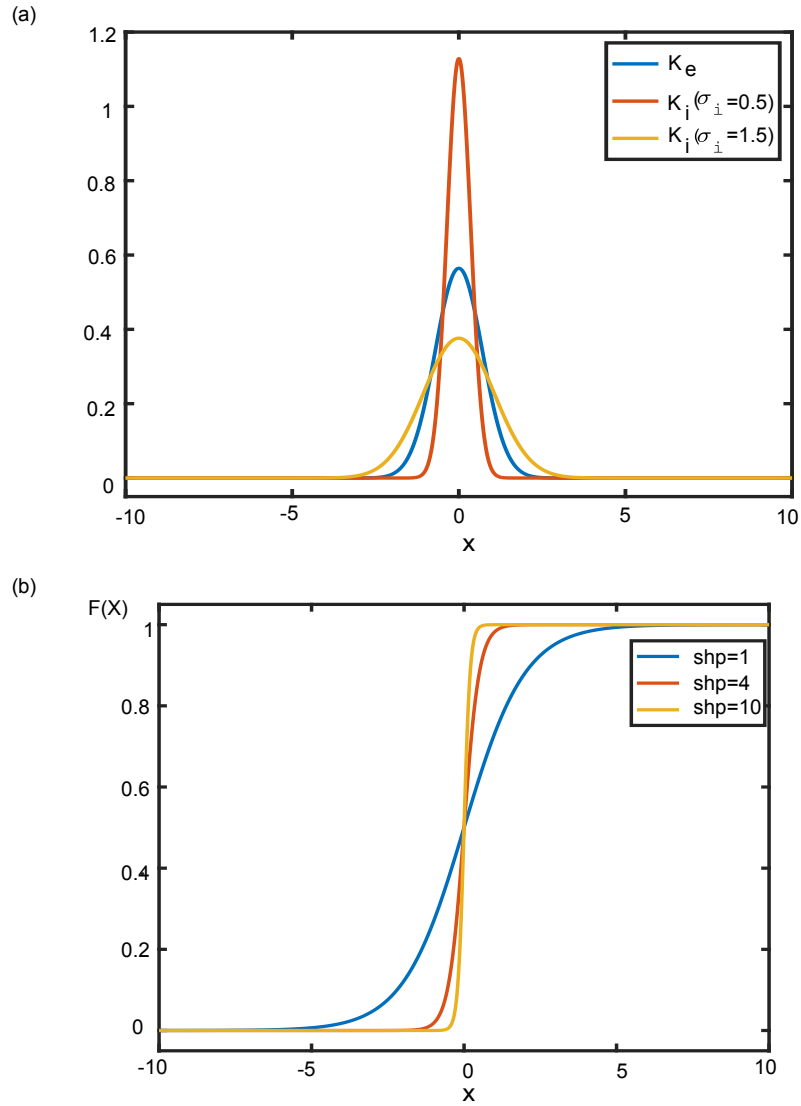


Figure 5: (a) Plot of K_e and K_i with $\sigma_i = 0.5$ and $\sigma_i = 1.5$ (b) $F(x) = 1/(1 + e^{-shp \cdot x})$ with increasing gain parameter: $shp = [1, 4, 10]$. For large value of shp , $F(x)$ can be approximated by the Heaviside function.

increases slowly. g_a (Fig8iv) has no visible effect on velocity since we started we very small value of u ($u \approx 0.02$). Only when u is large enough we will be able to see any effect. In

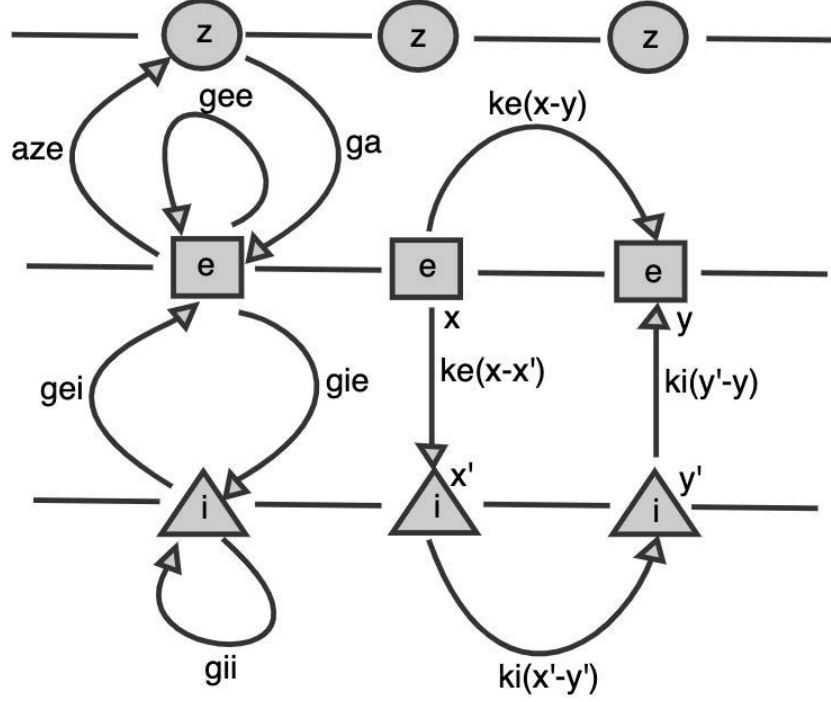


Figure 6: Schematic diagram of the spatially distributed network of the Wilson-Cowan equations.

Fig8v as the strength of excitation (d_e) increases, neurons start to fire faster, so velocity of the wave increases.

Next, we will compute the width of the traveling wave and study how it is affected by g_{ei} , σ_i , τ_i , g_a , d_e , d_i . $Width = t_{0100} - t_{100}$, where t_{0100} is the time at which u_{100} crosses the threshold ($u_{th} = 0.01$) from above and t_{100} is the time at which u_{100} crosses the threshold ($u_{th} = 0.01$) from below. The plots for width versus g_{ei} , σ_i , τ_i , g_a , d_e , d_i are computed using the data obtained from xppaut by integrating and ranging over the desired parameter.

Width (red curve) of the traveling wave decreases with increasing g_{ei} (Fig9i) and d_i (Fig9vi). This is because as the strength of inhibition increases the wave shuts down faster leading to decrease in the width of the wave. If there was no inhibition, the wave will have infinite width i.e. it will never die. So we can conclude $width \propto \frac{1}{g_{ei}}, \frac{1}{d_i}$. The width (red curve) increases with increasing τ_i (Fig9ii), because longer it takes for the inhibition to come

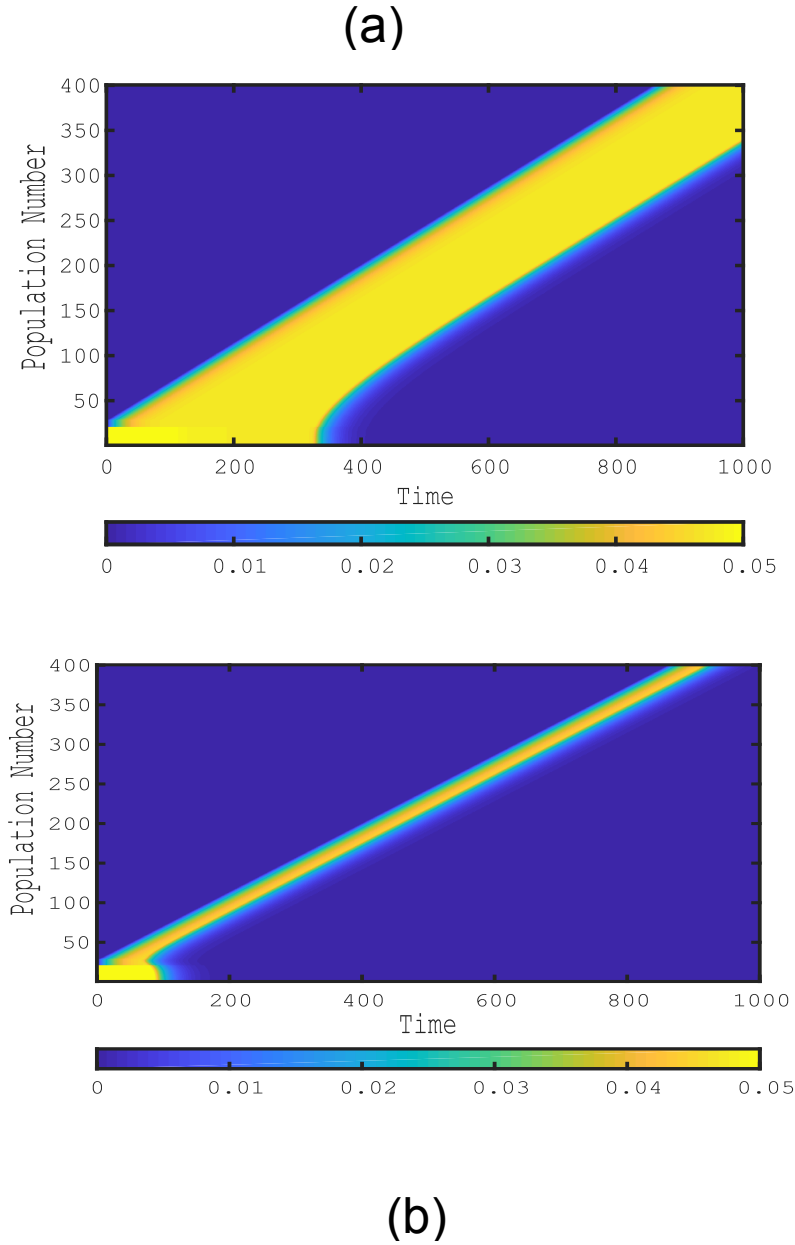


Figure 7: Space-time plot of the excitatory population with the smooth firing rate function for (a) $g_{ei} = 5$ and (b) $g_{ei} = 15$.

on, the longer it takes for the wave to shut off (or the width of the wave to decrease) i.e. width $\propto \tau_i$. In (Fig9v) the broader the reach of inhibition, the more sooner the wave dies off. Hence for larger values of σ_i , the width (red curve) goes to zero i.e. the wave shuts down

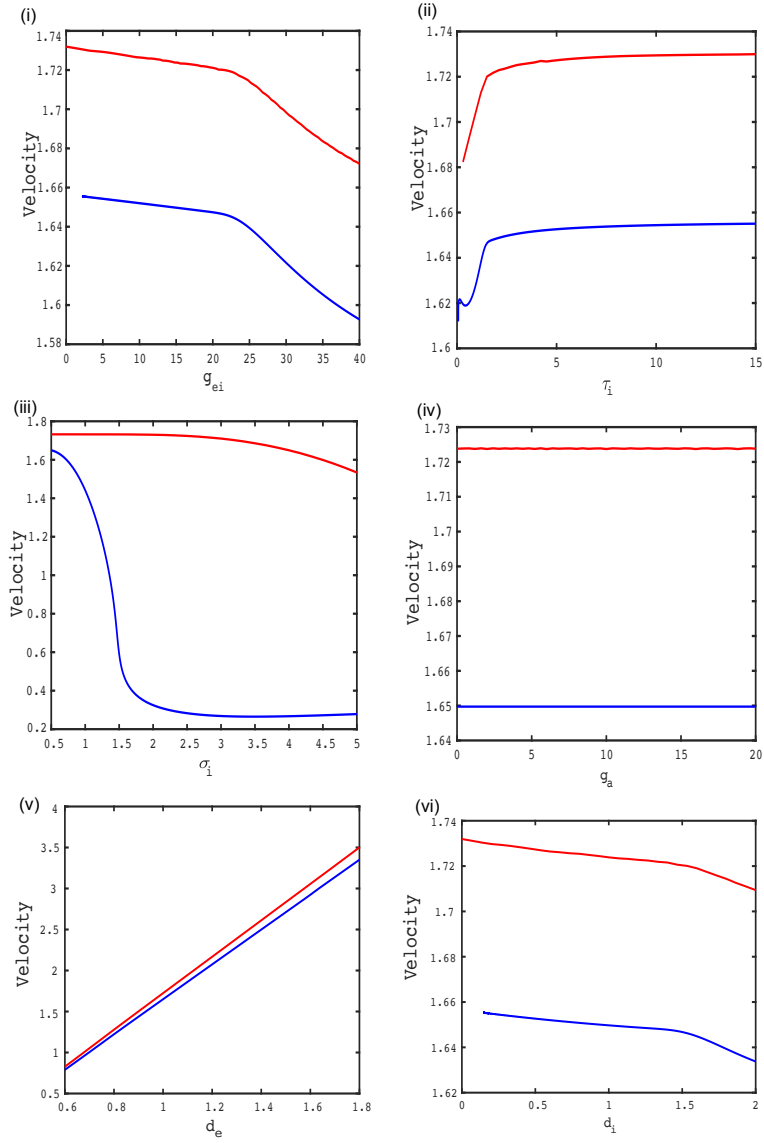


Figure 8: Figure (i) vel/g_{ei} , (ii) vel/τ_i , (iii) vel/σ_i , (iv) vel/g_a , (v) vel/d_e and (vi) vel/d_i are the velocity plots for smooth firing rate function (red curve) and Heaviside firing rate function (blue curve).

faster. Adaptation (g_a) does not have significant effect on the width of the wave (Fig9iv).

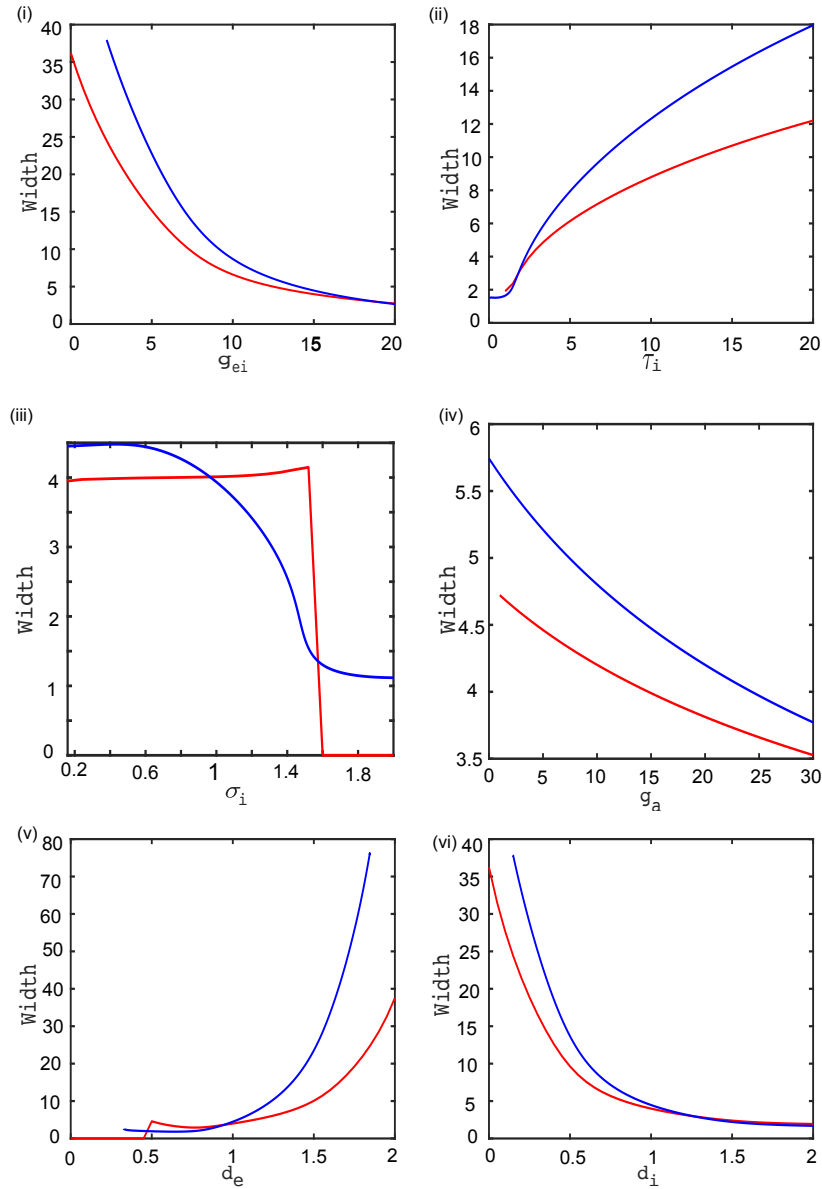


Figure 9: Figure (i) $width/g_{ei}$, (ii) $width/\tau_i$, (iii) $width/\sigma_i$, (iv) $width/g_a$, (v) $width/d_e$ and (vi) $width/d_i$ are the width plots for smooth firing rate function (red curve) and Heaviside firing rate function (blue curve).

Let us look at the $u-v$ (we take $u_{100}-v_{100}$) phase plane. In fig(10a) we study the $u-v$ phase plane as we increase $g_{ei} = [5, 10, 20, 30, 40, 50]$. The homoclinic orbits gets smaller

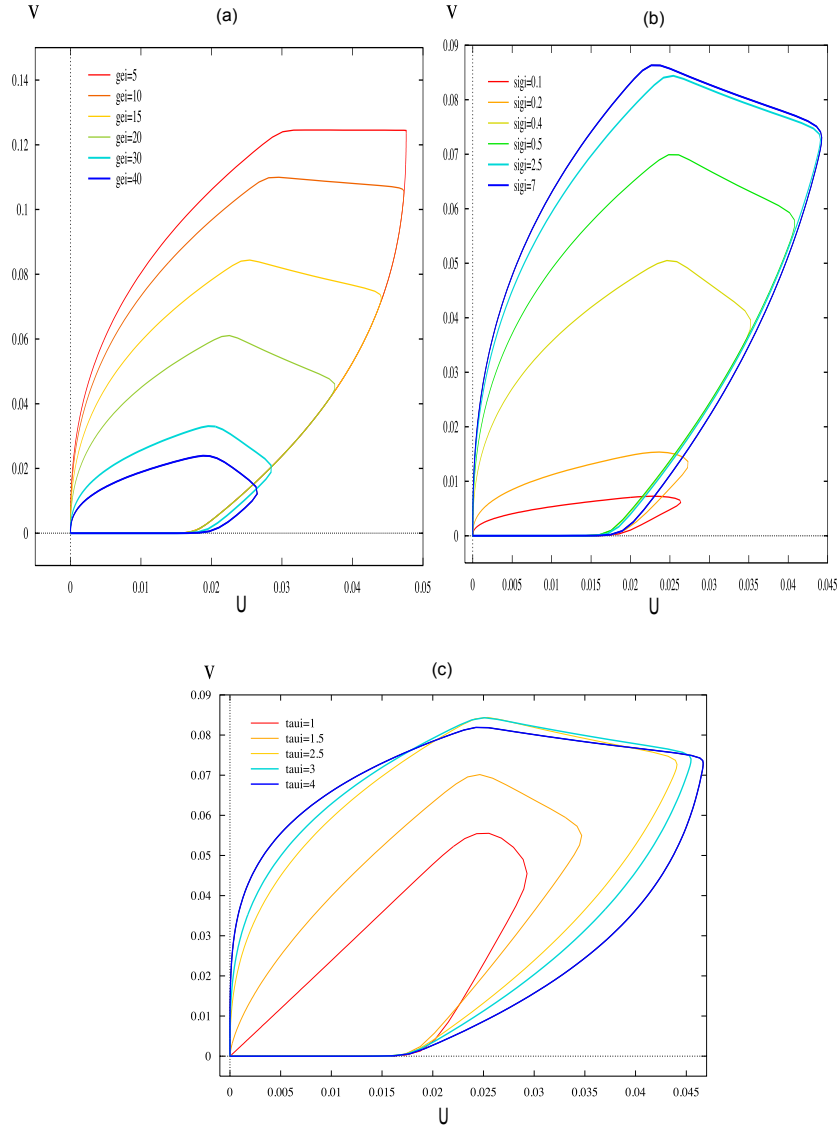


Figure 10: Homoclinic orbits in the $u-v$ phase plane for (a) varying g_{ei} , (b) varying σ_i and (c) varying τ_i .

as g_{ei} increases. This is because the more we increase the strength of inhibition, the more quickly the waves shut down ($\tau_i = 2.5$ and $\sigma_i = 0.5$ are fixed). In Fig(10b), we observe as $\sigma_i = [0.5, 1, 1.5, 2.5, 5]$ is increased for fixed $\tau_i = 2.5$ and $g_{ei} = 15$ the homoclinic orbits gets

larger in size. We can explain this by recalling that σ_i affects both excitation and inhibition. So as σ_i increases the excitation also increases and hence we need more inhibition to turn off the wave. Lastly in Fig(10c), for $\tau_i = [1, 1.5, 2, 4]$ and fixed $\sigma_i = 0.5$ and $g_{ei} = 15$, we observe the size of the homoclinic orbits increases with increasing τ_i . As τ_i increases (i.e. the time it takes for the inhibition to come on increases), the excitation can stay on for a longer time and hence the size of the homoclinic orbit increases. Next we will study the Wilson-Cowan equations with a Heaviside firing rate function.

3.0 WILSON-COWAN EQUATIONS WITH HEAVISIDE FIRING RATE FUNCTION

Let us consider the Heaviside firing rate function, $F(I) = \mathcal{H}(I)$. Thus, the Wilson-Cowan equations (2.1), (2.2) and (2.3) can be written as follows:

$$\frac{\partial u}{\partial t}(x, t) = -u(x, t) + \frac{1}{p} \mathcal{H}(p \cdot d_e \cdot g_{ee} \cdot K_e(x) * u(x, t) \tag{3.1}$$

$$- q \cdot d_i \cdot g_{ei} \cdot K_i(x) * v(x, t) + g_a \cdot z - \theta_e)$$

$$\tau_i \frac{\partial v}{\partial t}(x, t) = -v(x, t) + \frac{1}{q} \mathcal{H}(p \cdot d_e \cdot g_{ie} \cdot K_e(x) * u(x, t) \tag{3.2}$$

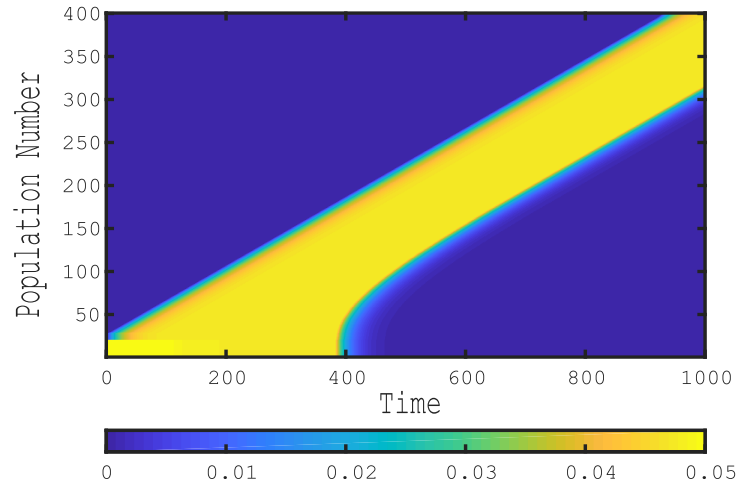
$$- q \cdot d_i \cdot g_{ii} \cdot K_i(x) * v(x, t) - \theta_i)$$

$$\tau_z \frac{\partial z}{\partial t}(x, t) = -z(x, t) + \mathcal{H}(p \cdot a_{ze} \cdot u(x, t) - \theta_z) \tag{3.3}$$

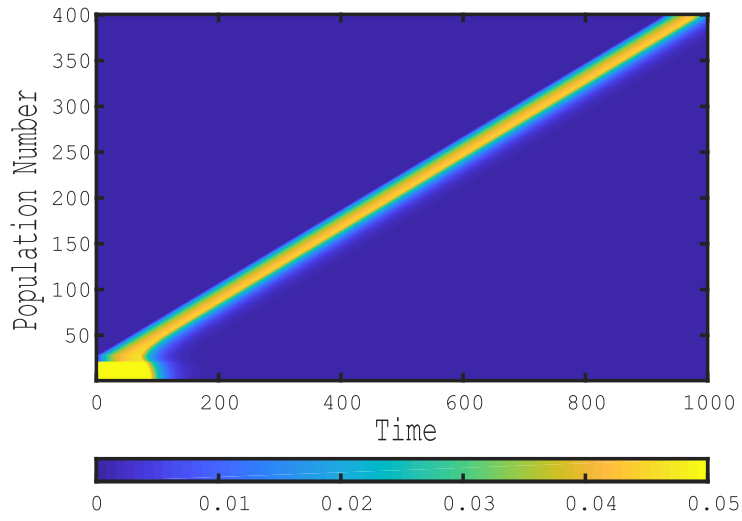
We are interested to know if we can obtain the same results we observed for smooth firing rate function. First we analyse the traveling wave arising in the excitatory population array as we change g_{ei} . Fig(11) shows that as we increase the inhibition (g_{ei}), the time for which a neuron fires decreases. This is similar to the result we see in case of the smooth firing rate function (Fig:7). In the coming sections we will look at the existence of the traveling wave and carry out stability analysis. We will use the Evans function for the stability analysis.

3.1 Existence of the traveling wave solution

We introduce the coordinate $\zeta = x + ct$, so that we have a traveling wave solution, where $c > 0$ is the unknown velocity of the wave. If we suppose solutions of the form $u(x, t) = u(\zeta)$, $v(x, t) = v(\zeta)$, $z(x, t) = z(\zeta)$, $\frac{\partial}{\partial t} = c \frac{d}{d\zeta}$ ($' = \frac{d}{d\zeta}$). In the phase space, the traveling waves



(a)



(b)

Figure 11: Space-time plot of the excitatory population with the Heaviside firing rate function for (a) $g_{ei} = 5$ and (b) $g_{ei} = 15$.

correspond to homoclinic (pulse) orbits. The system of equations 3.2,?? and 3.3 becomes:

$$\begin{aligned}
cu' &= -u + \frac{1}{p}\mathcal{H}(p \cdot d_e \cdot g_{ee} \cdot K_e * u - q \cdot di \cdot g_{ei} \cdot K_i * v - \theta_e - g_a \cdot z) \\
\tau_i cv' &= -v + \frac{1}{q}\mathcal{H}(p \cdot d_e \cdot g_{ie} \cdot K_e * u - q \cdot dig_{ii} K_i * v - \theta_i) \\
\tau_z cz' &= -z + \mathcal{H}(p \cdot a_{ze} \cdot u - \theta_z)
\end{aligned} \tag{3.4}$$

Denote:

$$\begin{aligned}
I_e(\zeta) &= p \cdot d_e \cdot g_{ee} \cdot k_e * u - q \cdot di \cdot g_{ei} \cdot k_i * v - \theta_e - g_a \cdot z \\
I_i(\zeta) &= p \cdot d_e \cdot g_{ie} \cdot k_e * u - q \cdot di \cdot g_{ii} \cdot k_i * v - \theta_i \\
I_z(\zeta) &= p \cdot a_{ze} \cdot u - \theta_z
\end{aligned}$$

a, b, d, e, f are chosen so that $I_e(0), I_e(a), I_i(b), I_i(d), I_z(e), I_z(f)$ are all zero. (Fig(12))

Note 1:

Any equation in system 3.4 has the general form:

$$c\tau g' = -g + (1/p)\mathcal{H}(I(\zeta)),$$

where $I(l) = I(k) = 0$, $I(\zeta) > 0$ for $l < \zeta < k$ and p is some scaling parameter. The solution to such an ODE is given by:

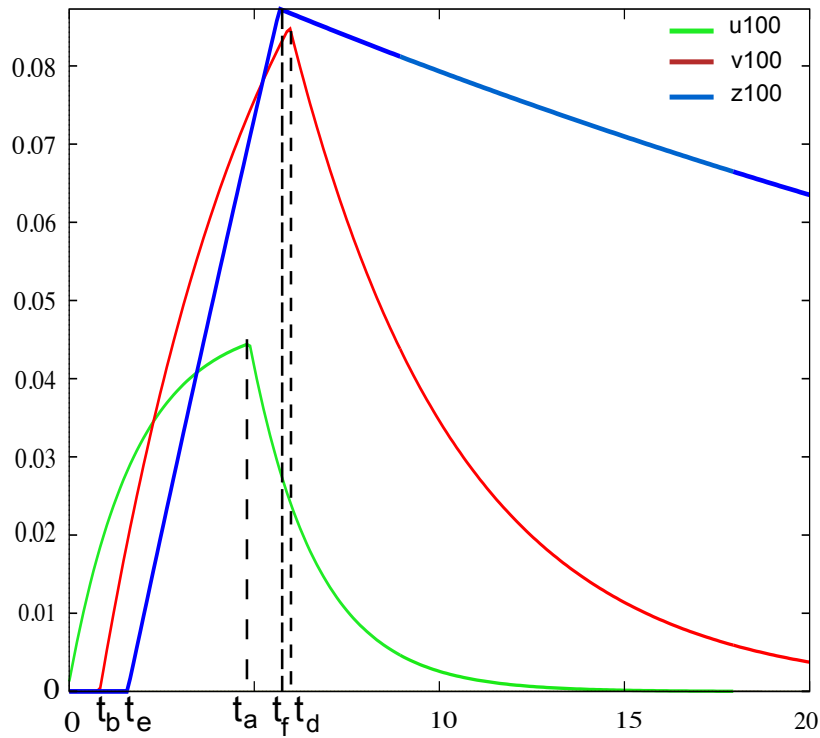
$$g(\zeta) = \begin{cases} 0 & \text{for, } \zeta \leq l \\ (1/p)(1 - e^{\frac{-(\zeta-l)}{c\tau}}) & \text{for, } l < \zeta < k \\ (1/p)(1 - e^{\frac{-(k-l)}{c\tau}})e^{\frac{-(\zeta-k)}{c\tau}} & \text{for, } \zeta \geq k \end{cases}$$

We can plug in the solutions to u, v, z obtained by using Note:1 into I_e, I_i, I_z to get:

$$\begin{aligned}
I_e(\zeta) &= d_e g_{ee} F(\zeta, \sigma, 1, c, 0, a) - d_i g_{ei} F(\zeta, \sigma, \tau_i, c, b, d) - \theta_e \\
I_i(\zeta) &= d_e g_{ie} F(\zeta, \sigma, 1, c, 0, a) - d_i g_{ii} F(\zeta, \sigma, \tau_i, c, b, d) - \theta_i \\
I_z(e) &= a_{ze}(1 - e^{\frac{(-e)}{c}}) - \theta_z \\
I_z(f) &= a_{ze}(1 - e^{\frac{(-a)}{c}})e^{\frac{(-f-a)}{c}} - \theta_z
\end{aligned} \tag{3.5}$$

where,

$$\begin{aligned}
F(\zeta, \sigma, \tau, c, \alpha, \beta) &= \frac{1}{\sqrt{\pi}\sigma} \int_{\alpha}^{\beta} e^{\frac{-(\zeta-\eta)^2}{\sigma^2}} (1 - e^{\frac{-(\eta-\alpha)}{c\tau}}) d\eta + \\
&\frac{1}{\sqrt{\pi}\sigma} \int_{\beta}^{\infty} e^{\frac{-(\zeta-\eta)^2}{\sigma^2}} (1 - e^{\frac{-(\beta-\alpha)}{c\tau}}) e^{\frac{-(\eta-\beta)}{c\tau}} d\eta
\end{aligned}$$



$$\begin{aligned}
 a &= (t_a)(\text{velocity}) \\
 b &= (t_b)(\text{velocity}) \\
 d &= (t_d)(\text{velocity}) \\
 e &= (t_e)(\text{velocity}) \\
 f &= (t_f)(\text{velocity}) \\
 \int_a^0 &= \int_a^a = \int_i^i (b) = \int_i^i (d) = \int_z^z (e) = \int_z^z (f) = 0
 \end{aligned}$$

Figure 12: u_{100} versus t (green), v_{100} versus t (red), z_{100} versus t (blue) plots. Scaled so that u_{100} starts at zero.

Using the system of equations (3.5) we can compute c, a, b, d, e, f by solving.

$$I_e(0) = 0$$

$$I_e(a) = 0$$

$$I_i(b) = 0$$

$$I_i(d) = 0$$

$$I_z(e) = 0$$

$$I_z(f) = 0$$

Now we use Auto to draw the bifurcation diagrams and study the behavior of velocity (c) and width (a) of the wave with respect to inhibition parameters like g_{ei} , τ_i , σ_i , g_a , d_i etc. Observe in fig(8) that the plot of velocity (blue curve) for the Heaviside firing rate function behaves very similar to the velocity plots (red curve) for the smooth firing rate function. Also, in fig(9) we notice that the plot for width (blue curve) versus the parameters g_{ei} , τ_i , σ_i , g_a , d_e and d_i mimics the same behavior as the width curve (red) in case of the smooth firing rate. As the Wilson-Cowan equations with Heaviside firing rate behave similar to the Wilson-Cowan equations with smooth firing rate, it is enough to study the Wilson-Cowan equations with Heaviside firing rate. In the next section we will look at the stability analysis of the traveling wave.

3.2 Stability analysis of Wilson-Cowan equations with Heaviside firing rate function

Let's consider the system in the traveling wave frame with $\zeta = x + ct$:

$$\begin{aligned}\frac{\partial u}{\partial t} + c \frac{\partial u}{\partial \zeta} &= -u + \frac{1}{p} \mathcal{H}(p \cdot d_e \cdot g_{ee} \cdot k_e * u - q \cdot di \cdot g_{ei} \cdot k_i * v - \theta_e - g_a \cdot z) \\ \tau_i \left(\frac{\partial v}{\partial t} + c \frac{\partial v}{\partial \zeta} \right) &= -v + \frac{1}{q} \mathcal{H}(p \cdot d_e \cdot g_{ie} \cdot k_e * u - q \cdot di \cdot g_{ii} \cdot k_i * v - \theta_i) \\ \tau_z \left(\frac{\partial z}{\partial t} + c \frac{\partial z}{\partial \zeta} \right) &= -z + \mathcal{H}(p \cdot a_{ze} u - \theta_z)\end{aligned}$$

Linearize this system about traveling wave (u_o, v_o) (let $u = u_o + \bar{u}, v = v_o + \bar{v}$), to obtain the following system:

$$\begin{aligned}\frac{\partial \bar{u}}{\partial t} + c \frac{\partial \bar{u}}{\partial \zeta} &= -\bar{u} + \frac{1}{p} \delta(I_e(\zeta)) (p \cdot d_e \cdot g_{ee} \cdot k_e * \bar{u} - q \cdot di \cdot g_{ei} \cdot k_i * \bar{v} - g_a \cdot \bar{z}) \\ \tau_i \frac{\partial \bar{v}}{\partial t} + \tau_i c \frac{\partial \bar{v}}{\partial \zeta} &= -\bar{v} + \frac{1}{q} \delta(I_i(\zeta)) (p \cdot d_e \cdot g_{ie} \cdot k_e * \bar{u} - q \cdot di \cdot g_{ii} \cdot k_i * \bar{v}) \\ \tau_z \frac{\partial \bar{z}}{\partial t} + \tau_z c \frac{\partial \bar{z}}{\partial \zeta} &= -\bar{z} + \delta(I_z(\zeta)) (p \cdot a_{ze} \cdot \bar{u})\end{aligned}$$

Let $\bar{u}(\zeta, t) = e^{\beta t} U(\zeta)$, $\bar{v}(\zeta, t) = e^{\beta t} V(\zeta)$, $\bar{z}(\zeta, t) = e^{\beta t} Z(\zeta)$ and use $\langle \delta(g(x)), \phi(x) \rangle = \int_{-\infty}^{\infty} \delta(g(x)) \phi(x) dx = \sum_i \frac{\phi(x_i)}{|g'(x_i)|}$. So in the sense of distribution $\delta(g(x)) = \sum_i \frac{\delta(x-x_i)}{|g'(x)|}$. Here x_i 's are non-repeating roots of g . So we get a simplified version:

$$\begin{aligned}\beta U + c \frac{dU}{d\zeta} + U &= \delta(\zeta) E^e(\zeta) + \delta(\zeta - a) E^e(\zeta) \\ \tau_i \beta V + c \tau_i \frac{dV}{d\zeta} + V &= \delta(\zeta - b) E^i(\zeta) + \delta(\zeta - d) E^i(\zeta) \\ \tau_z \beta Z + c \tau_z \frac{dZ}{d\zeta} + Z &= \delta(\zeta - e) E^z(\zeta) + \delta(\zeta - f) E^z(\zeta)\end{aligned} \tag{3.6}$$

Where:

$$E^e(\zeta) = \frac{1}{p \cdot |I_e(\zeta)'|} (p \cdot d_e \cdot g_{ee} \int_{-\infty}^{\infty} k_e(s-y)U(y)dy \quad (3.7)$$

$$- q \cdot d_i \cdot g_{ei} \int_{-\infty}^{\infty} k_i(\zeta-y)V(y)dy - g_a \cdot Z(\zeta))$$

$$E^i(\zeta) = \frac{1}{q \cdot |I_i(\zeta)'|} (p_e \cdot g_{ie} \int_{-\infty}^{\infty} k_e(\zeta-y)U(y)dy \quad (3.8)$$

$$- q \cdot d_i \cdot g_{ii} \int_{-\infty}^{\infty} k_i(\zeta-y)V(y)dy)$$

$$E^z(\zeta) = \frac{1}{|I_z(\zeta)'|} (p \cdot a_{ze} \cdot U(\zeta)) \quad (3.9)$$

We obtain $I'_e(\zeta)$, $I'_i(\zeta)$ and $I'_z(\zeta)$ by differentiating system 3.5 with respect to ζ .

Note2 : Any equation in system 3.6 has general form:

$$\alpha \frac{df}{d\zeta} + \beta f = \delta(\zeta - l)A(\zeta) + \delta(\zeta - k)B(\zeta)$$

The solution of such an equation is as follows:

$$f(\zeta) = \begin{cases} 0 & \text{if } \zeta \leq l \\ \frac{A(l)}{\alpha} e^{-\frac{(\zeta-l)\beta}{\alpha}} & \text{if } l < \zeta < k \\ \left(\frac{A(l)}{\alpha} e^{-\frac{(k-l)\beta}{\alpha}} + \frac{B(k)}{\alpha} \right) e^{-\frac{(\zeta-k)\beta}{\alpha}} & \text{if } \zeta \geq k \end{cases} \quad (3.10)$$

We get a system of six linear equations in terms of $E^e(0)$, $E^e(a)$, $E^i(b)$, $E^i(d)$, $E^z(e)$ and $E^z(f)$. To do this we plug in the values for U , V and Z using 3.10 in equations (3.7) to (3.9) and use $\zeta = 0, a$ for (3.7), $\zeta = b, d$ for (3.8) and $\zeta = e, f$ for (3.9). For each of the equations (3.7) to (3.9), we collect the terms together on one side of the equation, so as to equate the expression to zero. Now we have six linear equations with variables $E^e(0)$, $E^e(a)$, $E^i(b)$, $E^i(d)$, $E^z(e)$ and $E^z(f)$. We can rewrite them in a matrix form as follows:

$$\begin{bmatrix} a_{11} & a_{12} & a_{13} & a_{14} & a_{15} & a_{16} \\ a_{21} & a_{22} & a_{23} & a_{24} & a_{25} & a_{26} \\ a_{31} & a_{32} & a_{33} & a_{34} & a_{35} & a_{36} \\ a_{41} & a_{42} & a_{43} & a_{44} & a_{45} & a_{46} \\ a_{51} & a_{52} & a_{53} & a_{54} & a_{55} & a_{56} \\ a_{61} & a_{62} & a_{63} & a_{64} & a_{65} & a_{66} \end{bmatrix} \begin{bmatrix} E^e(0) \\ E^e(a) \\ E^i(b) \\ E^i(d) \\ E^z(e) \\ E^z(f) \end{bmatrix} = \begin{bmatrix} 0 \\ 0 \\ 0 \\ 0 \\ 0 \\ 0 \end{bmatrix}$$

where $(a_{ij})_{ij}$ are the coefficients obtained from equations (3.7) to (3.9). a_{ij} has the following values:

$$\begin{aligned}
a_{11} &= \left(\frac{1}{|I'_e(0)|c\tau_e} \right) (d_e g_{ee} \int_0^a k_e(0-y) e^{-\frac{y(\tau_e\beta+1)}{c\tau_e}} dy \\
&\quad + d_e g_{ee} \int_a^\infty K_e(0-y) e^{-\frac{a(\tau_e\beta+1)}{c\tau_e}} e^{-\frac{(y-a)(\tau_e\beta+1)}{c\tau_e}} dy) - 1 \\
a_{12} &= \left(\frac{1}{|I'_e(0)|c\tau_e} \right) (d_e g_{ee} \int_a^\infty K_e(0-y) e^{-\frac{(y-a)(\tau_e\beta+1)}{c\tau_e}} dy) \\
a_{13} &= \left(\frac{-1}{|I'_e(0)|c\tau_i} \right) (d_i g_{ei} \int_b^d k_i(0-y) e^{-\frac{(y-b)(\tau_i\beta+1)}{c\tau_i}} dy \\
&\quad + d_i g_{ei} \int_d^\infty K_i(0-y) (e^{-\frac{(d-b)\tau_i\beta+1}{c\tau_i}} e^{-\frac{(y-d)(\tau_i\beta+1)}{c\tau_i}} dy) \\
a_{14} &= \left(\frac{-1}{|I'_e(0)|c\tau_i} \right) (d_i g_{ei} \int_d^\infty K_i(0-y) e^{-\frac{(y-d)(\tau_i\beta+1)}{c\tau_i}} dy) \\
a_{15} &= 0 \\
a_{16} &= 0 \\
\\
a_{21} &= \left(\frac{1}{|I'_e(a)|c\tau_e} \right) (d_e g_{ee} \int_0^a k_e(a-y) e^{-\frac{y(\tau_e\beta+1)}{c\tau_e}} dy \\
&\quad + d_e g_{ee} \int_a^\infty K_e(a-y) e^{-\frac{a(\tau_e\beta+1)}{c\tau_e}} e^{-\frac{(y-a)(\tau_e\lambda+1)}{c\tau_e}} dy) \\
a_{22} &= \left(\frac{1}{|I'_e(a)|c\tau_e} \right) (d_e g_{ee} \int_a^\infty K_e(a-y) e^{-\frac{(y-a)(\tau_e\beta+1)}{c\tau_e}} dy) - 1 \\
a_{23} &= \left(\frac{-1}{|I'_e(a)|c\tau_i} \right) (d_i g_{ei} \int_b^d k_i(a-y) e^{-\frac{(y-b)(\tau_i\beta+1)}{c\tau_i}} dy \\
&\quad + d_i g_{ei} \int_d^\infty K_i(a-y) (e^{-\frac{(d-b)\tau_i\beta+1}{c\tau_i}} e^{-\frac{(y-d)(\tau_i\beta+1)}{c\tau_i}} dy) \\
a_{24} &= \left(\frac{1}{|I'_e(a)|c\tau_i} \right) (d_i g_{ei} \int_d^\infty K_i(a-y) e^{-\frac{(y-d)(\tau_i\beta+1)}{c\tau_i}} dy) \\
a_{25} &= g_a \left(\frac{e^{-\frac{a(\tau_e\beta+1)}{c\tau_e}}}{c\tau_e} \right) \\
a_{26} &= 0
\end{aligned}$$

$$\begin{aligned}
a_{31} &= \left(\frac{1}{|I'_i(b)|c\tau_e} \right) (d_e g_{ie} \int_0^a k_e(b-y) e^{\frac{-y(\tau_e\beta+1)}{c\tau_e}} dy \\
&\quad + d_e g_{ie} \int_a^\infty K_e(b-y) e^{\frac{-a(\tau_e\beta+1)}{c\tau_e}} e^{\frac{-(y-a)(\tau_e\beta+1)}{c\tau_e}} dy) \\
a_{32} &= \left(\frac{1}{|I'_i(b)|c\tau_e} \right) (d_e g_{ie} \int_a^\infty K_e(b-y) e^{\frac{-(y-a)(\tau_e\beta+1)}{c\tau_e}} dy) \\
a_{33} &= \left(\frac{1}{|I'_i(b)|c\tau_i} \right) (d_i g_{ii} \int_b^d k_i(b-y) e^{\frac{-(y-b)(\tau_i\beta+1)}{c\tau_i}} dy \\
&\quad + d_i g_{ii} \int_d^\infty K_i(b-y) (e^{\frac{-(d-b)\tau_i\beta+1}{c\tau_i}} e^{\frac{-(y-d)(\tau_i\beta+1)}{c\tau_i}} dy) - 1 \\
a_{44} &= \left(\frac{1}{|I'_i(b)|c\tau_i} \right) (d_i g_{ii} \int_d^\infty K_i(b-y) e^{\frac{-(y-d)(\tau_i\beta+1)}{c\tau_i}} dy) \\
a_{45} &= 0 \\
a_{46} &= 0
\end{aligned}$$

$$\begin{aligned}
a_{41} &= \left(\frac{1}{|I'_i(d)|c\tau_e} \right) (d_e g_{ie} \int_0^a k_e(d-y) e^{\frac{-y(\tau_e\beta+1)}{c\tau_e}} dy \\
&\quad + d_e g_{ie} \int_a^\infty K_e(d-y) e^{\frac{-a(\tau_e\beta+1)}{c\tau_e}} e^{\frac{-(y-a)(\tau_e\beta+1)}{c\tau_e}} dy) \\
a_{42} &= \left(\frac{1}{|I'_i(d)|c\tau_e} \right) (d_e g_{ie} \int_a^\infty K_e(d-y) e^{\frac{-(y-a)(\tau_e\beta+1)}{c\tau_e}} dy) \\
a_{43} &= \left(\frac{1}{|I'_i(d)|c\tau_i} \right) (d_i g_{ii} \int_b^d k_i(d-y) e^{\frac{-(y-b)(\tau_i\beta+1)}{c\tau_i}} dy \\
&\quad + d_i g_{ii} \int_d^\infty K_i(d-y) (e^{\frac{-(d-b)\tau_i\beta+1}{c\tau_i}} e^{\frac{-(y-d)(\tau_i\beta+1)}{c\tau_i}} dy) \\
a_{44} &= \left(\frac{1}{|I'_i(d)|c\tau_i} \right) (d_i g_{ii} \int_d^\infty K_i(d-y) e^{\frac{-(y-d)(\tau_i\beta+1)}{c\tau_i}} dy) - 1 \\
a_{45} &= 0 \\
a_{46} &= 0
\end{aligned}$$

$$\begin{aligned}
a_{51} &= \frac{1}{|I'_z(e)|c\tau_e} (a_{ze} e^{-\frac{e(\beta+1)}{c}}) \\
a_{52} &= 0 \\
a_{53} &= 0 \\
a_{54} &= 0 \\
a_{55} &= -1 \\
a_{56} &= 0 \\
a_{61} &= \left(\frac{1}{|I'_z(f)|c\tau_e} \right) a_{ze} e^{\frac{-a(\beta\tau_e+1)}{c\tau_e}} e^{\frac{-(f-a)(\beta\tau_e+1)}{c\tau_e}} \\
a_{62} &= \left(\frac{1}{|I'_z(f)|c\tau_e} \right) a_{ze} e^{\frac{-(f-a)(\beta\tau_e+1)}{c\tau_e}} \\
a_{63} &= 0 \\
a_{64} &= 0 \\
a_{65} &= 0 \\
a_{66} &= -1
\end{aligned}$$

Let us denote

$$\mathcal{E}(\beta) = \det \begin{bmatrix} a_{11} & a_{12} & a_{13} & a_{14} & a_{15} & a_{16} \\ a_{21} & a_{22} & a_{23} & a_{24} & a_{25} & a_{26} \\ a_{31} & a_{32} & a_{33} & a_{34} & a_{35} & a_{36} \\ a_{41} & a_{42} & a_{43} & a_{44} & a_{45} & a_{46} \\ a_{51} & a_{52} & a_{53} & a_{54} & a_{55} & a_{56} \\ a_{61} & a_{62} & a_{63} & a_{64} & a_{65} & a_{66} \end{bmatrix}$$

This system has a nontrivial solution if $\mathcal{E}(\beta) = 0$. We interpret $\mathcal{E}(\beta)$ as the Evans Function.

3.2.1 Evans function

The Evans function is an important tool for determining the stability of traveling waves. The computation of Evans-function allows us to locate any unstable eigenvalues (if they exist) of the linear operator. This in turn allows us to study the stability of a given wave and identify bifurcation points (loss of stability) as model parameters vary. Evans function

is a complex analytic function obtained by linearizing a system about its traveling wave and whose zeros give the eigenvalues of the linearized operator. It has the following properties:

1. The complex number β is an eigenvalue of the operator $\mathcal{L} \Leftrightarrow \mathcal{E}(\beta) = 0$.
2. The algebraic multiplicity of an eigenvalue is equal to the order of the zero of the Evans function.
3. As $\mathcal{E}(\beta)$ is complex analytic, there are at most finitely many eigenvalues within a disc.

A natural way to finding the zeros of $\mathcal{E}(\beta)$ is to write $\beta = a + ib$ and plot the zero contours of $real(\mathcal{E}(\beta))$ and $Img(\mathcal{E}(\beta))$ in the (a, b) plane, and look at the points of intersection.

In fig(13) we plot the real (red curve) and imaginary (blue curve) parts of the Evans function for $\sigma_i = 1.49$ (Fig(13a)), $\sigma_i = 1.502$ (Fig(13b)) and $\sigma_i = 1.52$ (Fig(13c)). We observe that as we increase σ_i (the spatial spread of inhibition) a pair of complex eigenvalues cross over from left to the right-half plane through the imaginary axis, thus illustrating Andronov-Hopf bifurcation (An Andronov-Hopf bifurcation arises when these two eigenvalues cross the imaginary axis because of a variation of the system parameters). In fig(13d) we track a root (in the fourth quadrant) of the Evans function as we change σ_i . We clearly notice that the real part of the Evans function (red curve) goes from negative to positive values, crossing zero at around $\sigma_i = 1.49$. This guarantees the existence of purely imaginary roots needed for the Andronov-Hopf bifurcation. Thus we can say our system undergoes dynamic instability with increasing σ_i . By dynamic instability we mean that a pair of complex eigenvalues crosses into the right hand plane on the imaginary axis so that the pulse begins to oscillate.

Let's go back to the Wilson-Cowan equations with a Heaviside firing rate and look at the array for the excitatory population as we change σ_i . Figure(14) gives the space-time plot of the excitatory population with the Heaviside firing rate for (a) $\sigma_i = 0.5$ (b) $\sigma_i = 1.467$ and (c) $\sigma_i = 1.47$. We observed oscillatory pattern when σ_i approaches the value 1.47. Hence we have oscillatory instability which was predicted by the stability analysis calculations above using the Evans Function. Now let's see if we observe similar oscillatory patterns in case of Wilson-Cowan equations with a smooth firing rate function. Figure(15) depicts the space-time plot of the excitatory population with the smooth firing rate function for (a) $\sigma_i = 0.5$, (b) $\sigma_i = 1.566$ and (c) $\sigma_i = 1.574$. We start to observe oscillatory patterns for σ_i around 1.56.

Hence the Wilson-Cowan equations with a smooth firing rate function also has oscillatory instability. Now as we the Wilson-Cowan model with the smooth firing rate function was a simplification of the spiking neuronal model, we can say that we must also have instability in the spiking model.

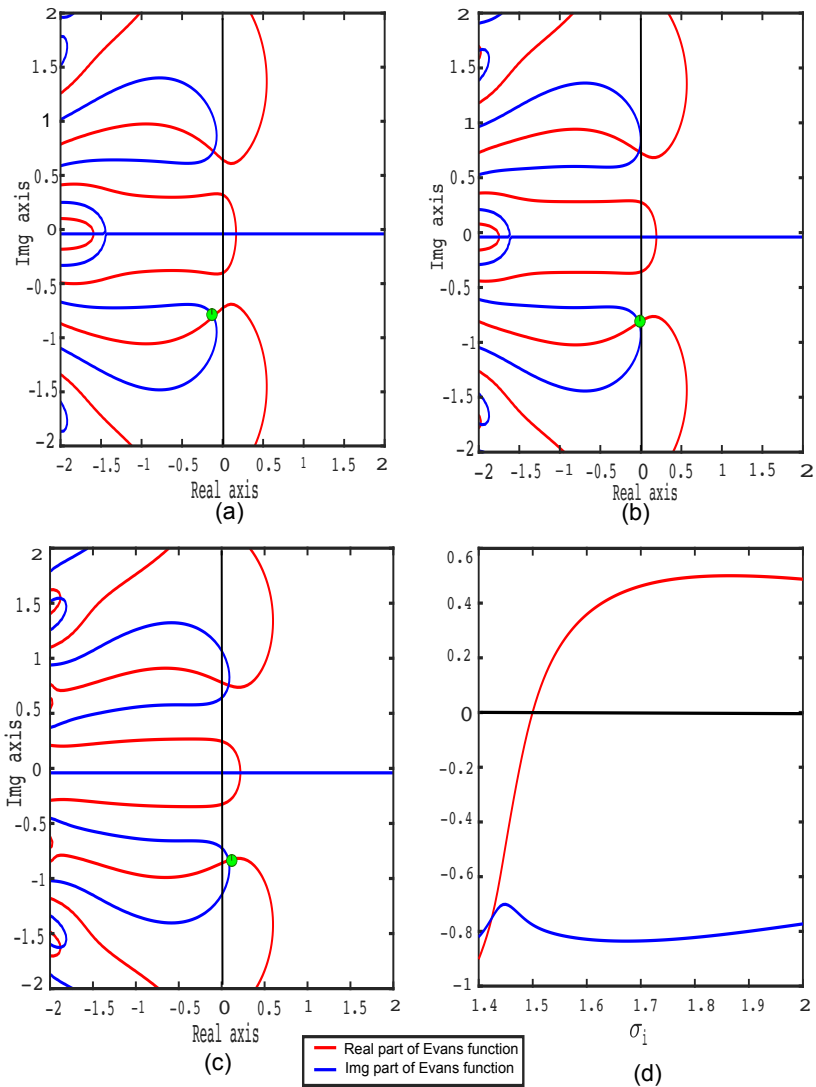


Figure 13: Plot of real and imaginary parts of the Evans function $\mathcal{E}(\beta)$ for the model with (a) $\sigma_i = 1.49$, (b) $\sigma_i = 1.502$ and (c) $\sigma_i = 1.52$ respectively. This illustrates a possibility of a dynamic instability with increasing σ_i as a pair of complex eigenvalues cross over to the right-hand plane through the imaginary axis. Figure (d) is the plot of Real part and Imaginary part of a root (green circle) of the Evans function vs σ_i . The graph of real part of Evans function crosses zero at approximately $\sigma_i = 1.5$.

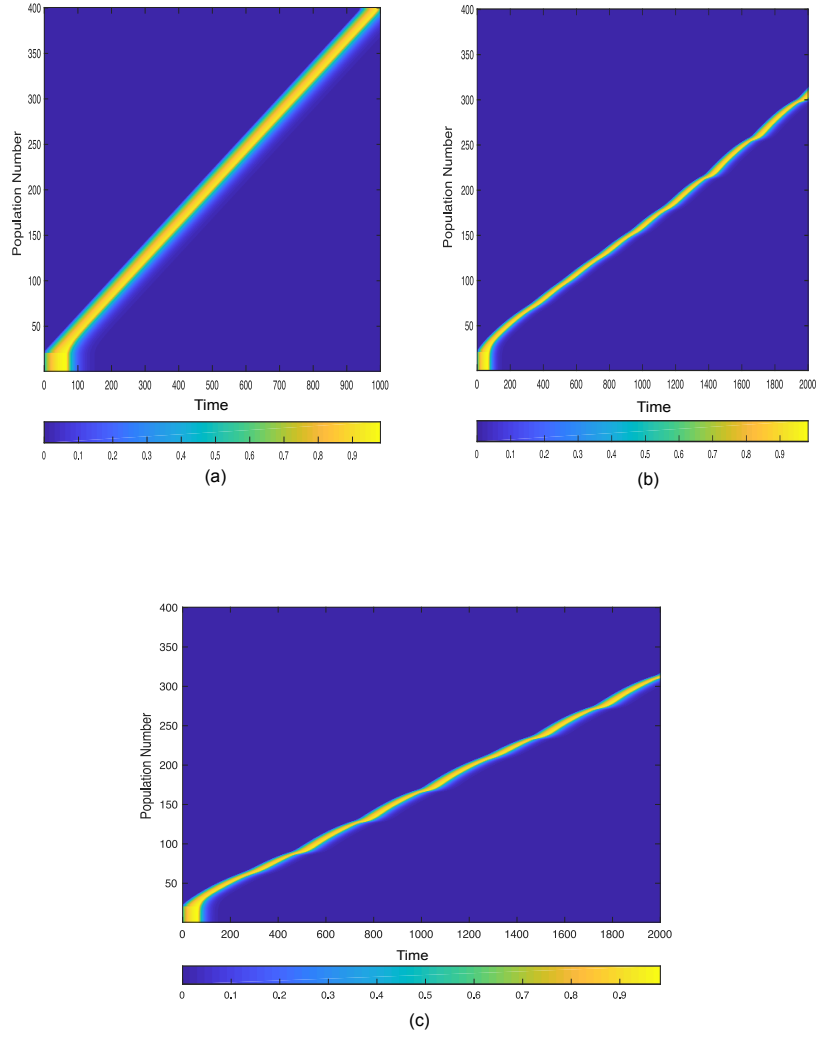


Figure 14: Space-time plot of the excitatory population with the Heaviside firing rate for (a) $\sigma_i = 0.5$, (b) $\sigma_i = 1.467$ and (c) $\sigma_i = 1.47$.

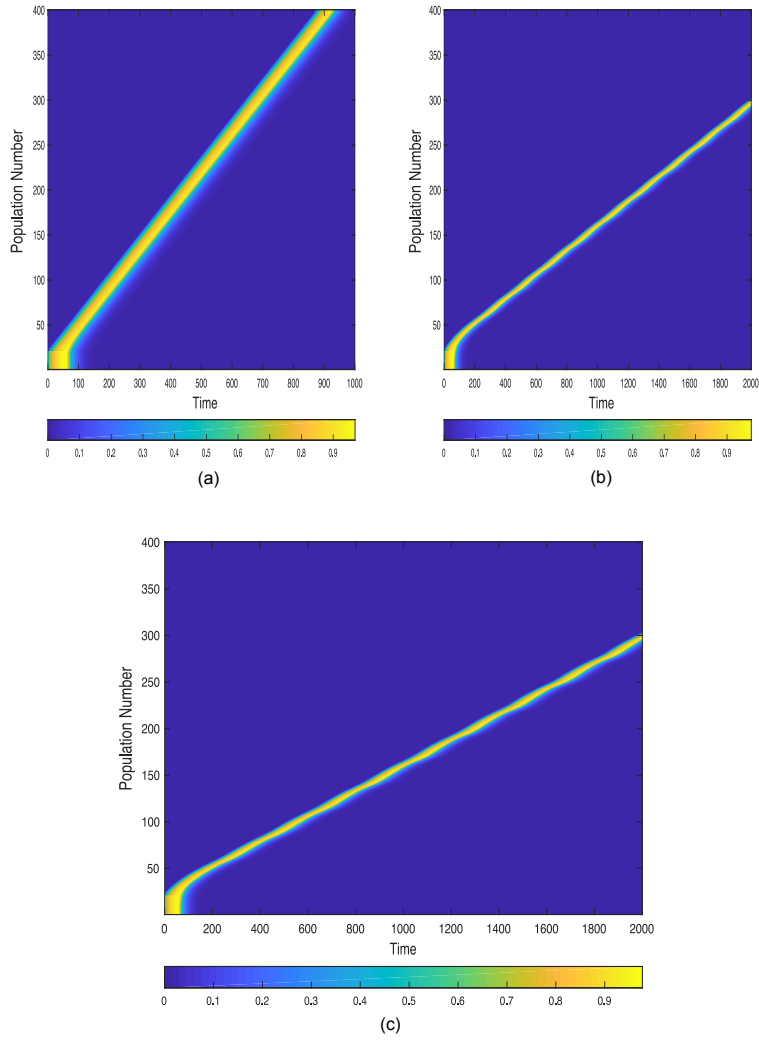


Figure 15: Space-time plot of the excitatory population with the smooth firing rate function for (a) $\sigma_i = 0.5$, (b) $\sigma_i = 1.566$ and (c) $\sigma_i = 1.574$.

4.0 CONCLUSIONS

- Inhibition controls the velocity and width of the traveling wave.
- When inhibition increases, the time for which a neuron fires decreases.
- When inhibition gets very small, adaptation controls the wave and we have pathologically big traveling waves.
- The stability analysis of the Wilson-Cowan equations with Heaviside firing rate function using Evans function showed that we have an Andronov-Hopf bifurcation at $\sigma_i \approx 1.49$. Hence, our system must undergo dynamic instability i.e. traveling waves must start to oscillate. To verify this we looked at the spatially distributed Wilson-Cowan equations with Heaviside and smooth firing rate function both. We observed that oscillatory patterns start to arise when σ_i approaches 1.5. As the Wilson-Cowan equations with the smooth firing rate function was a simplified version of the spiking neuronal model, we can conclude that the spiking neuronal model should also undergo dynamic instability.

BIBLIOGRAPHY

- [1] Coombes D, Owen MR (2004) Evans functions for integral neural field equations with Heaviside firing rate function. *SIAM J Appl Dyn Syst* 34:574–600
- [2] Harris JD, Ermentrout B. Traveling waves in a spatially- distributed Wilson–Cowan model of cortex: From fronts to pulses. *Physica D*. 2018;369:30–46.
- [3] Harris, J. Ermentrout, B. (2015) Bifurcations in the Wilson-Cowan equations with nonsmooth firing rate. *SIAM J. Appl. Dyn. Syst.* 14, 43–72.
- [4] L. Muller, F. Chavane, J. Reynolds, T.J. Sejnowski Cortical travelling waves: mechanisms and computational principles. *Nat. Rev. Neurosci.*, 19 (2018), pp. 255-268.
- [5] Pinto DJ, Ermentrout GB (2001a) Spatially structured activity in syn- aptically coupled neuronal networks: I. Travelling fronts and pulses *SIAM J Appl Math* 62:206–225
- [6] Pinto DJ, Ermentrout GB (2001b) Spatially structured activity in synap- tically coupled neuronal networks: II. Lateral inhibition and standing pulses. *SIAM J Appl Math* 62:226–243
- [7] Pinto, D.J., Patrick, S.L., Huang, W.C. Connors, B.W. Initiation, propagation, and termination of epileptiform activity in rodent neocortex in vitro involve distinct mechanisms. *J. Neurosci.* 25, 8131–8140 (2005).
- [8] Wester, J.C. Contreras, D. Columnar interactions determine horizontal propagation of recurrent network activity in neocortex *Journal of the Society for Neuroscience* 32(16), pp.5454–5471.